SOURCE AND PATH CALIBRATION IN REGIONS OF POOR CRUSTAL PROPAGATION USING TEMPORARY, LARGE-APERTURE, HIGH-RESOLUTION SEISMIC ARRAYS

John L. Nabelek[1], Jochen Braunmiller[1], Patrick W. Monigle[1], N. Seth Carpenter[1, 2], and W. Scott Phillips[3]

Oregon State University[1], Idaho National Laboratory[2], and Los Alamos National Laboratory[3]

Sponsored by Air Force Research Laboratory

Sponsored by National Nuclear Security Administration

Contract No. FA8718-09-C-004[1] and DE-AC52-06NA25396[3]
Proposal No. BAA09-28

ABSTRACT

Broadband seismic data acquired during the Hi-CLIMB experiment are used to study seismic events and path propagation in the Nepal Himalaya and the south-central Tibetan Plateau. The 2002–2005 experiment consisted of 233 stations along a dense 800 km linear north-south array extending from the Himalayan foreland into the central Tibetan Plateau. The main array was flanked by a 350 km x 350 km sub-array in southern Tibet and central and eastern Nepal. The dataset provides an opportunity to obtain seismic event locations for ground truth (GT) evaluation, to determine source parameters, and to study distance evolution of seismic coda for yield estimation in low Q regions.

In year three, we finalized the automated hypocenter locations in south-central Tibet. Refinements included an update of the model used for location based on high-quality manual P- and S-arrival picks from several strong events well recorded at close distances as well as the additional removal of spurious events. The database contains over 22,500 events from June 2004 to August 2005, which characterize the distributed seismicity in south-central Tibet. A subset of ~7,900 events with 25+ arrivals is considered well-located based on kilometer-scale differences relative to manually located events or InSAR constraints. Abundant seismicity north of the Yarlung Tsangpo Suture occurs primarily along upper crustal north-south trending extensional grabens and connecting strike-slip faults. Requiring distance to closest station ≤50 km and azimuthal gap ≤225° improves depth resolution considerably: events north of the southern Lhasa Block are generally shallow (<20km) while events south of it are either shallow or close to the Moho as observed in previous studies. The database contains over 400 GT5 candidate events; of these, almost 100 satisfy the $GT5_{95\%}$ criteria.

We continued analysis of seismicity along the Pumqu-Xianza Rift (PXR) (~30ºN, 88ºE) an area of known geothermal activity and high seismicity concentrating on 50 of the over 500 well-located events. Manual location places most events about 20-25 km west of the graben's eastern bounding fault and at ~10 km depth, which is consistent with depth estimates from regional moment tensor analysis. Moment tensors of the 11 best-resolved events ($3.2 \leq M_w \leq 4.5$) indicate rupture along a ~30º shallow westward dipping fault. Geometrically the fault's predicted surface location coincides with the most prominent fault scarp visible on Google Earth satellite imagery in the epicenter area lending support to this interpretation. In addition, imagery shows the N-S extent of seismicity coincides with the dimensions of a PXR graben segment. Observed strike-slip seismicity at the southern terminus of the segment relays lateral footwall motion to the east connecting to a prominent eastward dipping normal fault. Seismological data do not preclude rupture along a steeply (~60º) eastward dipping plane or along a listric fault near the base of the seismogenic crust, but satellite imagery does not support either scenario.

Resolving the 3-D P and S wave velocity and compositional structure is the focus of a recently initiated tomography effort aimed at complementing and expanding on the existing receiver function image of the collision zone; initial P-wave tomography results will be presented at the research review.

OBJECTIVES

The broadband Hi-CLIMB dataset covering the Himalayan-Tibetan collision zone is unique in its large aperture and dense station spacing. We study source and path calibration in regions of poor crustal propagation to enhance the monitoring community's capabilities to estimate magnitude and yield of future nuclear tests in low Q and highly scattering environments. We have three linked objectives for studying the seismicity: (1) obtain ground-truth seismic event hypocenters, (2) provide independent magnitude and depth estimates from modeling local and regional waveforms and (3) determine the distance evolution of seismic coda. In year three, efforts concentrated on (1) finalizing the 2004-2005 seismic event database and identifying GT5 events, (2) analyzing and interpreting seismicity associated with the Pumqu-Xianza Rift in southern Tibet, and (3) a task we just started, performing 3-D P- and S-velocity inversions for structure.

RESEARCH ACCOMPLISHED

Data

The 2002-2005 Hi-CLIMB broadband seismic experiment (Nabelek et al., 2009a) in Nepal and south-central Tibet occupied 233 sites. Station spacing along the ~800-km long north-south array covering the India-Eurasia collision zone from the Ganges foreland into the Tibetan Plateau was 3-4 km in the south and about 8 km north of the Yarlung-Tsangpo suture. Lateral deployments in Nepal and southern Tibet with 30-40 km station spacing improve earthquake location capabilities and provide wave propagation control for the foreland-plateau transition. Data were recorded continuously at 50 and 40 sps. The Hi-CLIMB data provide a unique opportunity to study small sized seismic events at unprecedented accuracy in central Asia. See Nabelek et al. (2009b; 2010) for a station map and additional network description.

Event Location

In year three, we finalized the automated hypocenter determinations in south-central Tibet. Results were presented by Carpenter et al. (2010). We used a low detection STA/LTA ratio of 3.0 and the association of 7+ phases to constitute an event to obtain a dataset as complete as possible. This approach resulted in an initial database of almost 110,000 declared events for the June 2004 to August 2005 period. We used post-processing filters to remove spurious detections and erroneous phase and event associations. Main considerations are (1) stations close to each other have to record an event and (2) stations close to the epicenter have to record an event. Initial arrival sets for a declared event could contain a significant number of wrongly associated detections resulting in a grossly incorrect location. The initial filter eliminates spurious detections or entire events based on (1). In later stages, we expect locations to be basically correct and thus require (2). Figure 1 shows step-by-step how filtering reduced the database' event count. The initial drop is due to implementing (1) and the second large drop is due to (2). Other steps corrected for wrong phase association caused by simultaneously occurring events in different locations within the Hi-CLIMB region, misplaced seismicity from the great 2004 Sumatra earthquake sequence, removal of glitches, and incorrect labeling of P- as S-arrivals and vice versa. The resulting database contains over 22,500 events (about 50 per day) with seven or more arrivals within 26°-36°N and 81.5°-93.5°E.

For several larger events, we manually picked P- and S-arrivals to refine the 1D velocity model for location and to evaluate automatic pick quality. We used two events from the Pumqu-Xianza Rift (PXR) with clear P and S onsets across the Hi-CLIMB array to refine the model because their hypocenters are well constrained and event-station paths sample southern Tibet resulting in a representative 1D model. Figure 2 shows the new (tib3p) and older (tibet3) 1D models and predicted (tib3p) and observed travel times for one event. The observed P arrivals are consistent with a simple two-crustal-layer over mantle model; shallow low-velocity layer agrees with receiver function analysis (Nabelek et al., 2009a) and waveform modeling (Baur et al., 2007). A single crustal S-velocity layer is required by the traveltime data (Figure 2) since S_n crossover distance is beyond the P_n crossover distance (at about 300 km). The upper mantle velocities in tib3p are based on the arrival times from the near-Moho events from the south. The model tib3p, which we uniformly used for locating the events, is strictly applicable only for the Lhasa block. South of the Yarlung-Tsangpo suture and north of the Bangong suture the velocity structure is clearly different, particularly the depth of Moho. We are now in the process of developing a 3D P and S velocity model and jointly locating the events.

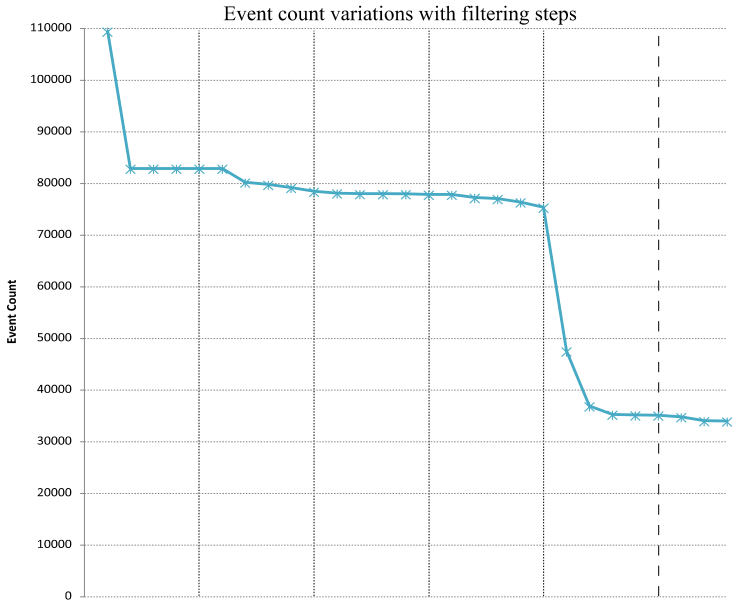

Figure 1. Change in number of events in the database with filter steps. Two sharp drops are due to requiring first stations close to each other and then stations close to an epicenter having to record an event, respectively. Plot includes all events defined by four and more arrivals. The final database for the Hi-CLIMB region with seven and more arrivals contains about 22,500 events.

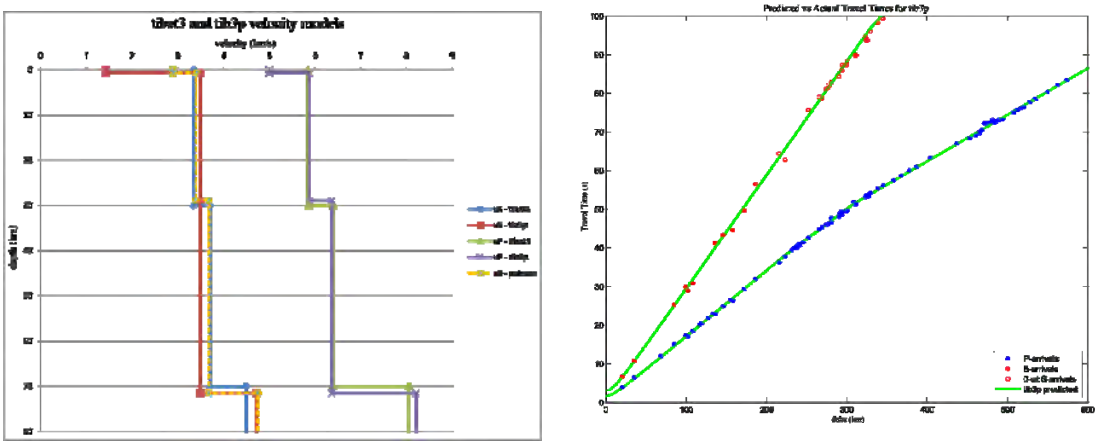

Figure 2. Left. New velocity model tib3p, used for final location of the Hi-CLIMB dataset, vs. earlier-used model tibet3. Right. Observed (dots) and predicted (green lines) travel times vs. offset for a manually picked PXR event. Predicted times based on tib3p. Red open circles are analyst-picked S-arrivals that were not used for location.

We manually picked P- and S-arrivals for 16 stronger events in southern Tibet to assess the quality of the automatic arrival-time picks used for location. Figure 3 shows differences between manual and automatic picks for P and S arrivals. At distances less than 300 km for P wave and less than 100 km for S waves the automatic picks generally agree with the manual picks at greater distances the automatic picks are generally late. We used this information to construct a distance weighting scheme giving full weight for P waves from 0° to 2° with a linear decreasing weight to 8°. For S waves, full weight was given up to 1° distance with a linear decrease to zero weight at 2°. However, event locations overall were not much affected by changes in the velocity model or the weighting. Event locations for manual and automatic picks are also very similar. For 16 manually picked events in southern Tibet, the mean epicenter difference is less than 3 km and for a set of 50 $2.1 \leq M_L \leq 4.8$ events in the PXR (Monigle et al., 2011), we

found a median difference of less than 2 km with a maximum difference of less than 8 km (Figure 4). The largest discrepancies occurred for events prior to the completion of the entire array.

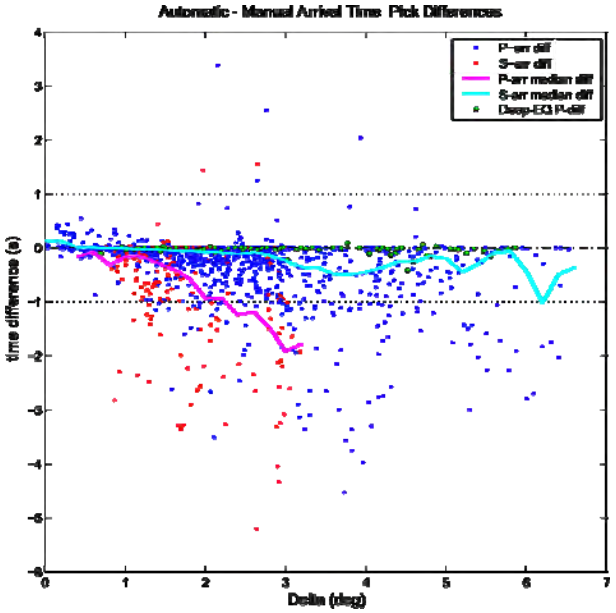

Figure 3. Manual-automatic arrival time differences for 16 stronger events in southern Tibet. P-differences in blue, S-differences in red, medians are solid lines (P: cyan, S: magenta). Note the small differences for a deep event (with impulsive P-onset) shown in green remain negligible for all observed distances.

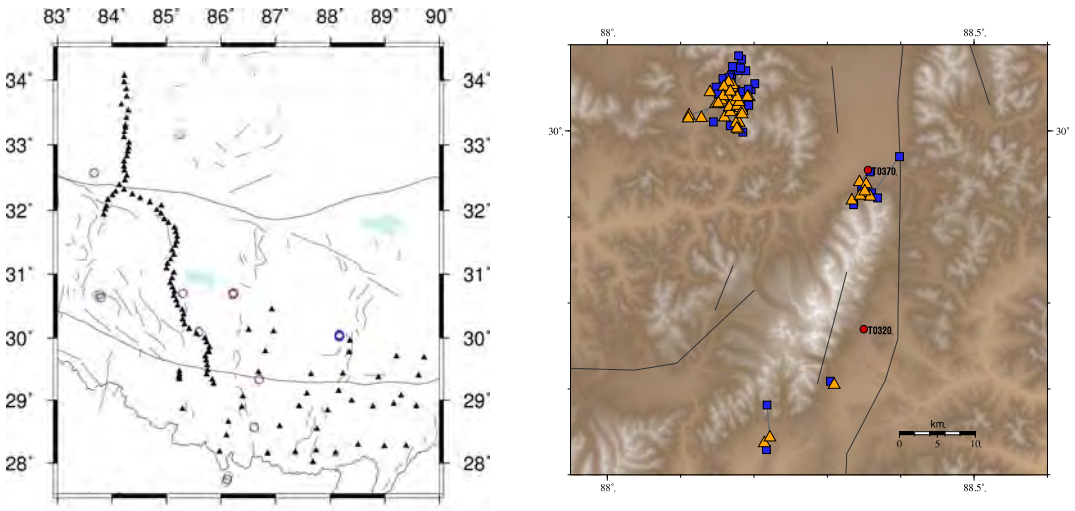

Figure 4. Left. The mean epicenter difference between automatic (red) and manually picked (blue) arrivals for 16 events in southern Tibet is less than 3 km. Right. Automatic (blue) and manual (orange) locations for 50 PXR events differ on average by less than 2 km and differences do not exceed 8 km.

The final database of over 22,500 events includes over 7,900 events (Figure 5) with at least 25 P and S arrivals, corresponding to well-located events throughout the map area. Of these, 4,500 have a local magnitude $M_L \geq 2.0$, which is a relevant cut-off for monitoring purposes. The locations based on automatic arrival time picks utilize S-arrivals, constraining the epicenters, and correlate with geologic structures seen in satellite imagery suggesting they are quite accurate. Seismicity is distributed throughout the study area. Most shallow seismicity north of the

Yarlung-Tsangpo Suture (YTS) is in an area not investigated by most other previous experiments. The most active source regions are north-south trending grabens in the Lhasa terrane. We located almost 10,000 events in the Payang Basin (near 30º-31ºN, 84ºE) following M_w>6 main shocks in July 2004 and April 2005, respectively. The distance from the Payang Basin to the closest stations is more than 100 km precluding consideration for GT-level locations (in addition to a one-sided station distribution). However, our locations for the two main shocks are consistent with InSAR derived fault area (Elliot et al., 2010). Vigorous seismicity (1,300+ events) was also observed from the vicinity of the Pumqu-Xianza Rift (~30ºN, 88ºE). There, due to close-by stations, differences between automatic and manual locations are only a few kilometers (Nabelek et al., 2009b); Figure 4 shows results for 50 $2.1 \le M_L \le 4.8$ events. Comparison with InSAR and manual locations suggests that epicenter uncertainties for most events in Figure 5 are probably less then 10 km.

Adding the requirements of distance to closest station $D_{min} \le 50$ km, azimuthal gap $Az \le 225°$, and $M_L \ge 2.0$ results in a high-quality subset of about 600 earthquakes. In addition to tighter clustering, event depths are now well resolved: events north of the southern Lhasa Block are generally shallow (<20km) while events south of it are either shallow or close to the Moho (Figure 5) as observed in previous studies (e.g., Langin et al., 2003; Monsalve et al., 2006; Liang et al., 2008). The events close to the Moho propagate across the entire array with mantle velocities and therefore their depth estimates are completely governed by the Moho depth. In tib3p the Moho is at a depth of 71 km but in reality it decreases south of the Yarlung-Tsangpo Suture to about 50 km under the Himalayas (Nabelek et al., 2009a). The depths of the deep events can be simply shifted to the appropriate hypocenter depth without altering the travel time fit by choosing the appropriate Moho depth for the given epicenter.

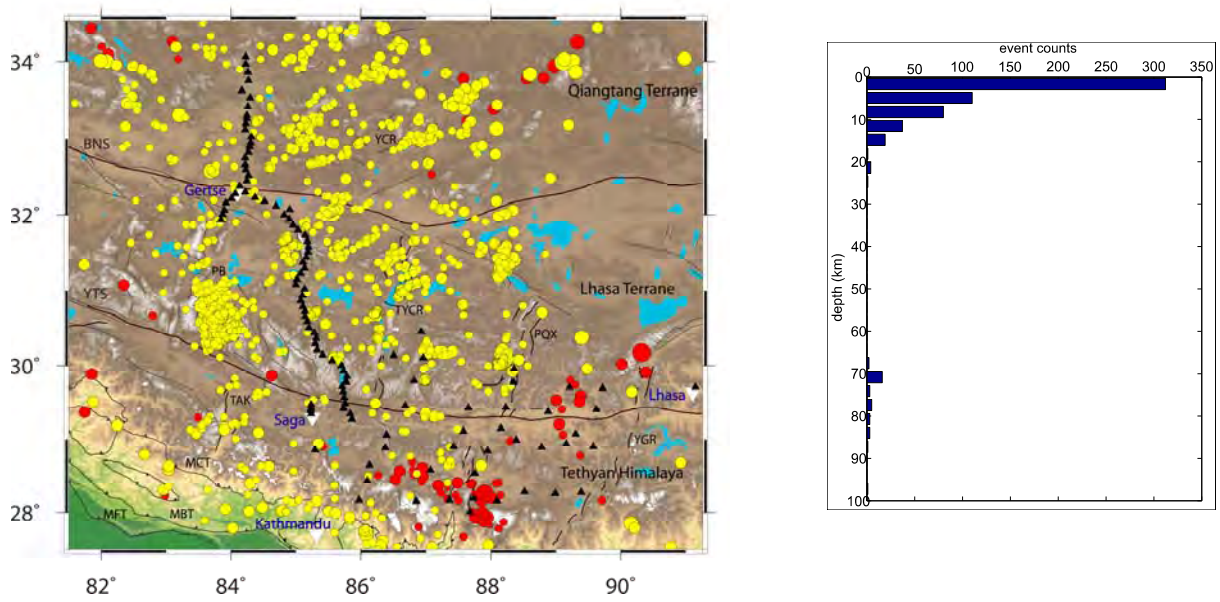

Figure 5. Left. Map of 7,900+ events with at least 25 P and S picks shows high-quality locations with distinct clustering. Colors distinguish crustal (yellow) from near-Moho events (red; z≥65km). Black triangles are June 2004 to August 2005 stations. PB is Payang Basin, PQX Pumqu-Xianza Rift, and YTS Yarlung-Tsangpo Suture. Red events outside network, e.g. in the Qiangtang terrane, have poorly determined depth. Right. Requiring $D_{min} \le 50$ km, gap ≤225°, and $M_L \ge 2.0$ results in ~600 events with well-constrained depth. The depth distribution is bimodal as observed previously; deep events are observed beneath the Tethyan Himalaya (mainly between ~86-88ºE) and near the Yadong-Gulu Rift.

Local Magnitude $M_L(P)$

We determined local magnitude from maximum seismogram amplitudes of a short time window around the P arrival correcting for expected S-to-P amplitude ratio differences of $(v_p/v_s)^3 \approx 5$. We call the corrected magnitude $M_L(P)$ (Nabelek et al., 2010). On average, $M_L(P)$ is consistent with moment magnitude M_w from regional moment tensors (Baur, 2007) and matches teleseismic Global CMT M_w and USGS NEIC body wave magnitude m_b (Figure 6). Event

$M_L(P)$ are medians based on at least 3 observations within 600 km distance and a minimum signal-to-noise ratio of 3 after Wood-Anderson filtering resulting in over 4,000 events with $M_L(P)$. The frequency-magnitude plot suggests completeness for $M_L(P)\geq 3.3$ within 600 km and $M_L(P)\geq 2.0$ within 150 km of the array.

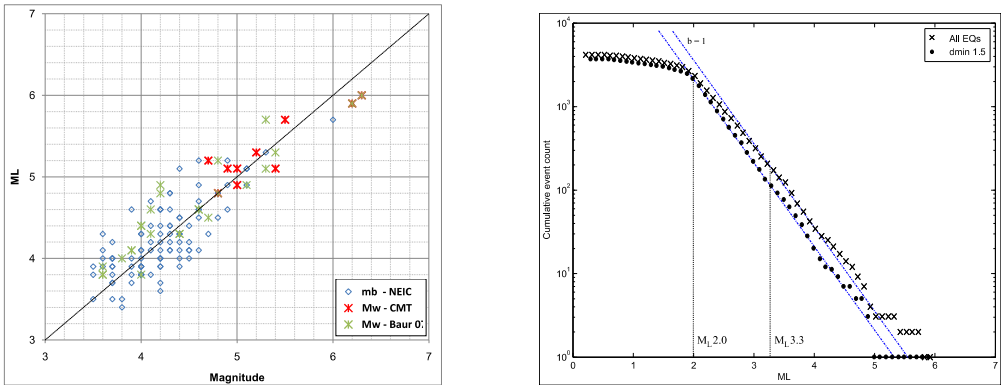

Figure 6. Left. $M_L(P)$ versus NEIC m_b, Global CMT and regional moment tensor (Baur, 2007) M_w. Right. Frequency-magnitude relation for 4,000+ events within 600 km of the array and at least 3 magnitude observations with a minimum signal-to-noise ratio of 3 per event.

Ground Truth Events

We applied the Bondar et al. (2004) criteria to identify candidate events for the seismic event ground truth (GT) database. Our Hi-CLIMB dataset includes 406 events recorded by 10 or more stations within 250 km distance, with an azimuthal gap of 110º or less, and at least one station within 30 km from the epicenter. Of these, 93 events are at $GT5_{95\%}$-level (they additionally have a secondary azimuthal gap of 160º or less and were recorded by P/P_n beyond 250 km distance), 5 events are $GT5_{90\%}$ (not satisfying the secondary gap criterion). All 406 events are shown in Figure 7. Table 1 includes all 48 GT5 (44 $GT5_{95\%}$) candidates above the monitoring relevant $M_L(P)\geq 2.0$ threshold.

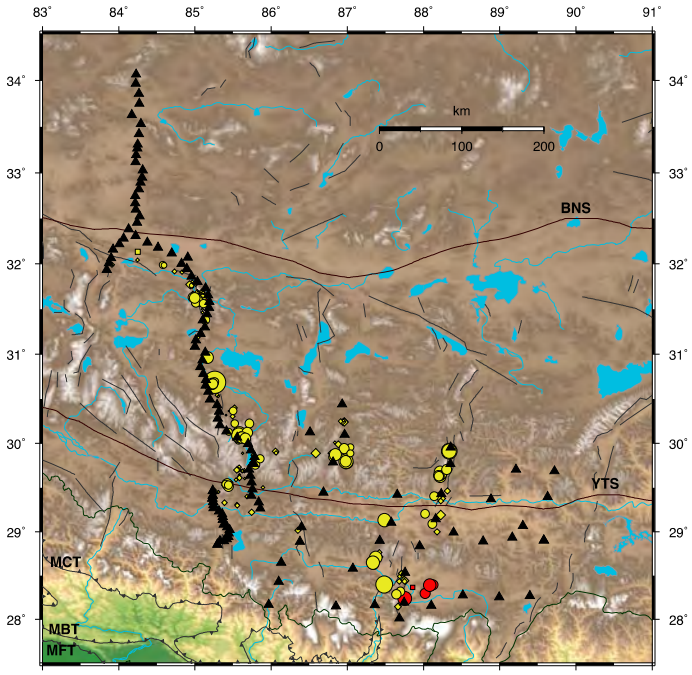

Figure 7. Map of 406 GT5 candidate events. Circles are 93 $GT5_{95\%}$, squares 5 $GT5_{90\%}$, and diamonds 308 other candidates (all 308 lack P/P_n beyond 250 km distance; 276 satisfy the secondary gap criterion). At $M_L(P)\geq 2.0$, the map shows 44 $GT5_{95\%}$, 4 $GT5_{90\%}$ and 11 other events. Colors are as in Figure 5.

Nine manually located GT5 events (marked "&" in Table 1) are listed in Table 2. For these, the median difference between manual and automatic pick locations is <1.5 km with a median depth difference of 6 km; depth based on automatic picks is consistently shallower. For event #22, moment tensor inversion resulted in a double-couple strike-slip source mechanism at 15 km depth with roughly N-S and E-W trending nodal planes (Monigle et al., 2011). Parameter uncertainties (~20º for strike, dip, and rake and ±10 km for depth) are large due to small event size (M_w=3.2, M_L(P)=3.1). The only event listed in the USGS NEIC and the ISC catalogs is event #38. The NEIC and ISC locations are about 13 km and over 30 km, respectively, south-southwest of our location. Manual locations with Hi-CLIMB data (ours and Griffin et al. 2011) are within a few km of the automated location. Moment tensor analysis reveals a well-constrained double-couple strike-slip mechanism at 4 km depth with an E-W trending σ_3-axis. Magnitude estimates for the event are similar (M_L(P)=4.7, M_w=4.4 vs. m_b(NEIC)=4.6 and m_b(ISC)=4.3).

Table 1. $GT5_{95\%}$ and $GT5_{90\%}$ ("*" in first column) candidate events with magnitude $M_L \geq 2.0$. "&": Nine manually located events, see Table 2; their median epicenter difference is <1.5 km and manual hypocenters are generally deeper with a median difference of 6 km.

Event (#)	Date (M/D/Y)	Time (UTC)	Latitude (°N)	Longitude (°E)	Depth (km)	M_L(P)
1	06/17/04	07:00:23.8	31.600	85.054	0.0	2.2
2	06/26/04	01:26:36.9	31.586	85.015	0.0	2.0
3	07/02/04	00:45:10.8	31.608	85.043	7.0	2.0
4	07/22/04	17:34:29.7	28.397	88.123	74.3	2.1
5	08/02/04	21:48:29.7	28.299	88.021	75.5	2.2
6	08/03/04	09:36:06.2	29.774	86.983	13.7	2.2
7	08/05/04	19:09:27.2	29.784	87.002	3.1	2.3
8	08/13/04	17:10:42.6	29.132	87.488	2.7	2.8
9	08/16/04	10:20:55.0	29.545	85.426	0.1	2.3
10	08/16/04	13:46:55.4	29.520	85.442	11.9	2.1
11&	09/04/04	17:36:54.2	30.105	85.584	0.8	3.2
12	09/15/04	04:36:26.7	30.095	85.577	8.6	3.0
13	10/22/04	03:28:42.5	28.707	87.374	0.0	2.7
14	11/19/04	05:10:21.0	31.635	84.972	6.1	2.0
15	12/08/04	22:48:37.3	29.801	86.984	0.0	3.0
16	12/08/04	22:57:20.2	29.803	86.980	0.5	2.4
17	12/15/04	00:03:07.2	28.393	88.082	71.6	2.6
18*&	12/29/04	03:24:12.4	29.935	88.347	5.6	2.1
19&	01/01/05	22:46:22.7	29.917	88.336	4.2	3.4
20*	01/03/05	06:14:43.0	29.939	88.353	5.3	2.2
21*	01/07/05	00:20:03.1	29.935	88.350	7.1	2.0
22&	01/08/05	12:51:10.1	29.914	88.336	3.9	3.1
23	02/16/05	02:33:55.7	30.966	85.165	4.3	2.6
24	02/20/05	23:41:13.3	29.646	88.207	0.8	2.2
25&	02/22/05	23:38:26.8	29.629	88.217	0.7	2.5
26	02/23/05	02:03:45.6	29.643	88.227	0.0	2.1
27&	02/23/05	03:30:09.5	29.681	88.218	0.0	2.5
28	02/23/05	19:53:04.2	29.635	88.207	0.0	2.2
29	03/19/05	09:30:47.1	29.946	86.959	4.9	2.2
30*	04/03/05	23:08:32.8	32.135	84.252	13.8	2.0
31	04/21/05	20:28:47.0	31.628	84.996	20.2	2.2
32	04/30/05	03:43:11.0	29.645	88.192	0.8	2.1
33	05/03/05	08:51:23.5	28.239	87.754	82.8	3.0
34	05/10/05	09:33:55.3	28.627	87.345	13.2	2.2
35	05/10/05	21:47:53.2	28.648	87.335	0.6	2.5
36	05/11/05	00:45:35.7	30.670	85.234	7.2	2.8
37	05/11/05	01:51:49.0	30.668	85.234	6.1	2.1
38&	05/11/05	04:13:00.3	30.688	85.262	1.6	4.7
39	05/11/05	06:37:07.3	28.650	87.338	10.0	2.8
40	05/11/05	08:25:44.7	30.672	85.230	5.1	2.5
41	05/11/05	23:58:15.9	29.876	86.843	0.0	2.6
42&	06/04/05	20:44:15.7	29.709	88.304	0.4	2.2
43	06/09/05	18:53:58.8	30.123	85.685	0.0	2.2
44	06/16/05	18:34:32.2	28.287	87.644	65.9	2.0
45&	07/06/05	03:11:02.9	28.398	87.485	66.7	3.6
46	07/28/05	00:21:38.1	30.070	85.618	7.3	2.4
47	07/29/05	05:06:03.1	30.670	85.236	12.6	2.1
48	08/15/05	10:13:46.3	30.058	85.664	0.8	2.3

Table 2. Manual locations for 8 $GT5_{95\%}$ and 1 $GT5_{90\%}$ candidate events. Numbers "#" are as in Table 1. "&" are PXR events, "*" is $GT5_{90\%}$. Moment tensor analysis was successfully performed for #22 and #38.

Event (#)	Date (M/D/Y)	Time (UTC)	Latitude (°N)	Longitude (°E)	Depth (km)	$M_L(P)$
11	09/04/04	17:36:54.4	30.091	85.593	7.3	3.2
18*&	12/29/04	03:24:12.1	29.928	88.352	8.3	2.1
19&	01/01/05	22:46:22.2	29.919	88.334	9.9	3.4
22&	01/08/05	12:51:09.1	29.925	88.345	10.3	3.1
25&	02/22/05	23:38:26.3	29.637	88.214	4.7	2.5
27&	02/23/05	03:30:09.1	29.643	88.222	7.6	2.5
38	05/11/05	04:13:00.3	30.671	85.243	7.6	4.7
42&	06/04/05	20:44:15.2	29.705	88.310	7.9	2.2
45	07/06/05	03:11:02.8	28.376	87.515	70.2	3.6

Low-Angle Normal Faulting in the Pumqu-Xianza Rift

We continued detailed analysis of seismicity in the Pumqu-Xianza Rift (PXR) focusing on 50 events recorded between July 2004 and June 2005 when close sites T0370 and T0320 (Figure 8) were operating. The database contains about 350 events with 25 or more automatic P- and S-picks slightly west of the PXR near 30.0ºN and 88.2ºE. From these, we relocated the 40 largest events ($M_L(P)\geq3.2$) using manual P- and S-picks. The automated database also includes events near T0370 and T0320 (Figure 8). We selected 10 stronger events ($2.1\leq M_L(P)\leq3.4$) from this group to verify their location accuracy; six of these events satisfy GT5-criteria (Table 2, marked "&" in Table 1). A comparison between automated and manual locations (Figure 4) illustrates the high quality of locations from automatic picks. The azimuthal gap requirement precludes GT5 consideration for the main event cluster.

The manual locations cluster tightly west of the central PXR (Figure 8) and at about 10 km depth. The hypocenters are constrained by phase picks from close stations and are consistent with ~12 km depth (uncertainties of about ±3 km) estimated from moment tensor analysis (Monigle et al., 2011). All main cluster mechanisms are consistent with N-S oriented normal faulting on a ~30º west-dipping fault. Rupture on the shallow dipping plane is geometrically consistent with event locations at 10 km depth about 20-25 km west of the eastern boundary fault of the central PXR. The eastern boundary fault is a prominent feature on Google satellite imagery. The north-south extent of the main cluster appears bound by a segment boundary within the PXR system with activity confined to what we term the Qingdu Segment (~29.95º-30.15ºN). We favor this internally consistent interpretation. We cannot, however, rule out rupture along a steeply east-dipping fault or on a listric west-dipping fault, though satellite imagery does not show any significant surface features in support of these alternatives. We observe no hypocenter migration throughout the sequence and events remain near ~10 km depth, which for this geothermally active region is possibly near the bottom of the seismogenic zone, suggestive of a driving mechanism from below. We have one strike-slip mechanism for the largest event of the cluster just south of T0370. These events likely represent lateral motion on a short transform fault connecting the shallow west-dipping normal fault north of T0370 with an east-dipping fault southeast of T0370. The east-dipping range-bounding fault is a prominent feature on Google satellite images.

Global source parameter compilations of continental normal faulting earthquakes (e.g., Jackson and White, 1987; Collettini and Sibson, 2001) include only few documented cases of rupture along faults dipping less than 40º. The most plausible scenario for the PXR events is rupture along a ~30º-dipping low-angle normal fault assuming the small fault patches at ~10 km depth connect to the prominent Qingdu Segment scarp at the surface. For a vertical orientation of the minimum stress axis σ_3, frictional reactivation of a 30º-dipping fault is possible but requires a high ratio of the maximum horizontal stress σ_1 to σ_3 and a relatively low friction coefficient $\mu<0.6$ (Collettini and Sibson, 2001) or a slight stress-axis rotation.

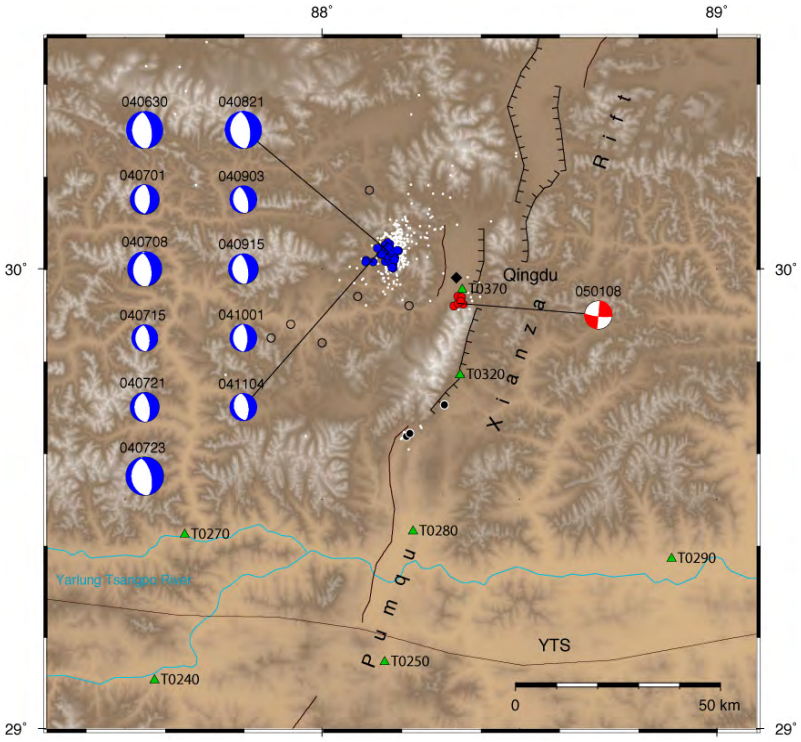

Figure 8. Map of the central PXR showing manual locations for 50 events; blue are events west of the rift, red near station T0370 and black south of T0320. White dots are epicenters from automatic picks (Carpenter et al., 2010); their north-south extent coincides with the Qingdu Segment of the PXR. Green triangles are Hi-CLIMB stations. Diamond is town of Qingdu. Open circles are NEIC locations for 6 events that all relocated into the blue cluster. Fault plane solutions from moment tensor analysis are identified by event date (YYMMDD). From Monigle et al. (2011).

Tomographic Imaging Using P and S Waves

Resolving the 3-D P and S wave velocity and compositional structure is the focus of a recently initiated tomography effort aimed at complementing and expanding on the existing receiver function image of the collision zone; initial P wave tomography results will be presented at the research review.

CONCLUSIONS AND RECOMMENDATIONS

The Hi-CLIMB broadband seismic dataset provides a unique opportunity to determine ground truth event locations, regional velocity models, earthquake source parameters for moderate-sized events, and coda distance decay. Implementation of refined clean-up modules resulted in a database of more than 22,500 seismic events in the Hi-CLIMB study area with locations determined by automatic phase picks. Manual locations of a small subset of events in southern Tibet reveal a non-systematic, a-few-kilometer-scale difference between locations based on automatic and manual phase picks. Applying additional requirements on the station distribution results in a high-quality subset of events with resolved hypocenters that show a bimodal depth distribution. We identified about 400 GT5-candidate events of which 98 satisfy the GT5 criteria at the 95% or 90% confidence level. We performed precise hypocenter locations and regional moment tensor determinations to characterize the vigorous seismic activity near the Pumqu-Xianza Rift resulting in manual GT5-locations. We plan to obtain further improvements in event location and characterization through tomographic imaging and attenuation analysis; these efforts are currently in their initial stages. The GT5 locations and moment tensors will contribute to SLBM tomographic efforts, allow evaluation of depth for crustal models, and enhance model accuracy throughout central and southern Asia and, in general, will contribute to the National Nuclear Security Administration (NNSA) Knowledge Base.

REFERENCES

Baur, J. (2007). Seismotectonic analysis of the Himalayan-Tibetan collision zone from regional seismic moment tensor analysis with Hi-CLIMB data, *M.Sc. thesis, Oregon State University, Corvallis, Oregon*, 276 pp.

Bondar, I., S. C. Myers, E. R. Engdahl, E. A. Bergman (2004). Epicentre accuracy based on seismic network criteria, *Geophys. J. Int*. 156: 483–496, doi: 10.1111/j.1365-246X.2004.02070.x, 2004.

Carpenter, S., J. Nábělek, and J. Braunmiller (2010), South-central Tibetan seismicity from HiCLIMB seismic array data, *Eos Trans. Am. Geophys. Union*, 91 (52), Fall Meet. Suppl., Abstract T43B-2223.

Collettini, C., and R. H. Sibson (2001), Normal faults, normal friction?, *Geology*, 29, 927-930.

Elliot, J. R., R. J. Walter, P. C. England, J. A. Jackson, Z. Li, and B. Parsons (2010), Extension on the Tibetan plateau: Recent normal faulting measured by InSAR and body wave seismology, *Geophys. J. Int.*, 183, 503-535, doi: 10.1111/j.1365-246X.2010.04754.x.

Griffin, J. D., R. L. Nowack, W.-P. Chen, and T.-L. Tseng (2011), Velocity structure of the Tibetan lithosphere: Constraints from P-wave travel times of regional earthquakes, *Bull. Seismol. Soc. Am.*, 101: 1938–1947.

Jackson, J. A., and N. J. White (1989), Normal faulting in the upper continental crust: observations from regions of active extension, *J. Struct. Geol.*, 11: 15–36.

Langin, W. R., L. D. Brown, and E. A. Sandvol (2003), Seismicity of central Tibet from project INDEPTH III seismic recordings, *Bull. Seismol. Soc. Am.* 93: 2146–2159.

Liang, X., S. Zhou, Y. J. Chen., G. Jin, L. Xiao, P. Liu, Y. Fu, Y. Tang, X. Lou, and J. Ning (2008), Earthquake distribution in southern Tibet and its tectonic implications, *J. Geophys. Res.*, 113: B12409, doi: 10.1029/2007JB005101.

Monigle, P., J. L. Nábělek, J. Braunmiller, and S. Carpenter, Low-angle normal faulting in the Pumqu-Xianza Rift, Tibet (2011), submitted to *Geophys. Res. Lett*.

Monsalve, G., A. Sheehan, V. Schulte-Pelkum, S. Rajaure, M. R. Pandey, and F. Wu (2006), Seismicity and one-dimensional velocity structure of the Himalayan collision zone: Earthquakes in the crust and upper mantle, *J. Geophys. Res.*, 111, B10301, doi: 10.1029/2005JB004062.

Nábělek, J., G. Hetényi, J. Vergne, S. Sapkota, B. Kafle, M. Jiang, H. Su, J. Chen, B.-S. Huang, and the Hi-CLIMB Team (2009a). Underplating in the Himalaya-Tibet collision zone revealed by the Hi-CLIMB experiment, *Science* 325: 1371, doi: 10.1126/science.1167719.

Nábělek, J. L., J. Braunmiller, and W. Scott Phillips (2009b). Source and path calibration in regions of poor crustal propagation using temporary, large-aperture, high-resolution seismic arrays, in *Proceedings of the 2009 Monitoring Research Review: Ground-Based Nuclear Explosion Monitoring Technologies*, LA-UR-09-05276, Vol. 1, pp. 158-165.

Nábělek, J. L., S. Carpenter, P. Monigle, J. Braunmiller, and W. Scott Phillips (2010). Source and path calibration in regions of poor crustal propagation using temporary, large-aperture, high-resolution seismic arrays, in *Proceedings of the 2010 Monitoring Research Review: Ground-Based Nuclear Explosion Monitoring Technologies*, LA-UR-10-05578, Vol. 1, pp. 150–160.